

Comparative Study of IgG Binding to Proteins G and A: Nonequilibrium Kinetic and Binding Constant Determination with the Acoustic Waveguide Device

K. Saha, F. Bender, and E. Gizeli*

Institute of Biotechnology, University of Cambridge, Tennis Court Road, Cambridge CB2 1QT, United Kingdom

The aim of this work was to measure and compare the binding constants of antibody immunoglobulin G (IgG) to bacterial cell wall proteins, streptococcal protein G and *Staphylococcus aureus* protein A, using an acoustic wave sensor. Devices, which used shear-horizontal acoustic waves propagating in a waveguide configuration at 108 and 155 MHz, were employed in the detection of apparent IgG binding constants at the solid–liquid interface in the range of 6.7–667 nM IgG. Real-time data during IgG–protein G and IgG–protein A binding yielded apparent association constants of 3.29×10^4 and $8.02 \times 10^3 \text{ M}^{-1} \text{ s}^{-1}$ leading to equilibrium constants of 1.13×10^8 and $2.90 \times 10^7 \text{ M}^{-1}$, respectively. The measured apparent rate constants are consistent with literature reports of higher affinity of protein G for IgG. Furthermore, protein binding through the Fc region of IgG is suggested to occur below 333 nM, while different mechanisms are suggested to occur above 333 nM. For the first time, nonequilibrium studies of IgG–protein G and A binding at a solid–liquid interface has yielded valuable quantitative kinetic information about binding mechanisms. The promise of this detection method is shown by providing quick determination of binding constants with low sample volumes.

The binding between a ligand and a receptor is of ever-increasing importance in the pharmaceutical industry, sensor, and scientific communities. Understanding the full implications of the human genome project and the emerging field of proteomics have introduced new needs to probe further millions of protein interactions. Rapid, low-cost methods of biological binding analysis are furthermore vital in escalating environmental concerns and defense applications in light of rising biological defense strategies. From a scientific viewpoint, mechanisms behind the reversible binding of ligands to receptors are a result of weak, noncovalent interactions between them, including ionic interaction, hydrogen bonds, van der Waals forces, and hydrophobic interactions—al areas of current biochemical research.¹

Ligand–receptor binding events occur both in solution and at interfaces, notably on cell membranes. Immunological antibody–

antigen reactions and enzymatic reactions in the blood are examples of solution-phase binding. At interfaces, immunological reactions such as antigen presentation by major histocompatibility complexes (MHC) or signal transduction events are well-investigated examples. It is equally possible to measure, in principle, the binding parameters of immunological reactions in solution and at interfaces in their native environment and geometry. However, such ideal characterization of a given ligand–receptor pair is not always a straightforward experimental approach. In solution measurements of binding parameters, well-defined and thermodynamically equilibrated boundary conditions occur such as an isotropic distribution of the binding partners, well-characterized translational and rotational diffusion constants, and homogeneous microenvironments of binding sites.² However, a major problem of measuring binding parameters in solution concerns the difficulty in separating unbound from bound binding partners. Therefore, tedious washing and separation procedures may be needed. Furthermore, in situ monitoring of reaction kinetics is often not possible.²

Current means that avoid these problems and satisfy the need for high-throughput rapid analysis involve interactions of ligands with receptors at liquid–solid interfaces. A surface enables easy spatial separation of bound compounds from the free compounds in solution. Solid interfaces also allow the employment of surface-sensitive techniques such as optical evanescent wave techniques, electrochemical impedance spectroscopy, and acoustic techniques. An acoustic technique with a functionalized sensor surface, where receptors for Fc fragment of antibodies are immobilized, is used in this work. This technique is minimally invasive to the binding, requires no labeling, and allows real-time measurement over very small amounts of sample volumes.

The acoustic technique employed is based on an acoustic waveguide geometry first used in biosensors in 1992.³ Briefly, this geometry comprises a surface acoustic wave device where an electric potential applied to piezoelectric substrate via interdigitated transducers (IDTs) creates a surface-localized, shear-horizontal-polarized acoustic wave (Figure 1). The phase and amplitude of the SH-SAW are measured with time through

* Corresponding author. E-mail: e.gizeli@biotech.cam.ac.uk.

(1) Hall, Z. W. *An Introduction to molecular neurobiology*; Sinauer Associates: Sunderland, MA, 1992.

(2) Duschl, C. In *Biomolecular sensors*; Gizeli, E., Lowe, C. R., Eds.; Taylor and Francis: London, 2002, pp 87–120.

(3) Gizeli, E.; Goddard, N. J.; Lowe, C. R.; Stevenson, A. C. *Sens. Actuators, B* 1992, 6, 131–137.

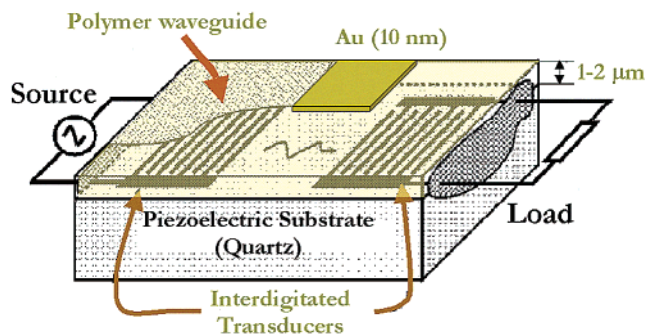


Figure 1. Schematic of acoustic waveguide device. Drawing not to scale.

electrical connections to the IDTs. A polymer layer deposited on the device surface serves as an acoustic waveguide by localizing acoustic energy of waves in the substrate away from the bulk and onto the surface. Additional layers, such as the gold layer in Figure 1, serve as convenient platforms to develop biorecognition surfaces. All sensing occurs in a surface volume within which there is significant acoustic displacement. Such displacement occurs when the oscillation of the device surface is coupled into the surface medium and induces an oscillation in the liquid. This oscillation does not extend throughout the bulk of the liquid but is damped within a small distance of the surface, the penetration depth (~ 50 nm). Acoustic wave propagation is sensitive to mass, viscoelastic, and electrical changes within penetration depth.⁴ During the last 10 years, the waveguide device has been optimized, both theoretically^{5,6} and experimentally,^{3,7–9} and successfully tested to sense mass changes occurring in biological layers deposited on the device surface.^{3,10–13} Furthermore, the mass sensitivity of this technique is comparable to optical techniques such as surface plasmon resonance and orders of magnitude higher than quartz crystal microbalance sensors.⁴

Characterization of ligand–receptor binding primarily involves determination of three properties: the equilibrium binding constant and the two reaction rate constants of association and dissociation. The equilibrium binding constant, K , indicates the ratio between bound and unbound ligands for a given concentration of receptor under steady-state conditions. The two reaction rate constants, k_a and k_d , determine the association rate of complex formation and dissociation rate of its disintegration, respectively. Knowledge of K ($K = k_a/k_d$) gives thermodynamic, global information on the binding behavior at equilibrium condition, while knowledge of k_a and k_d reveals kinetic understanding of molecular mechanisms.

- (4) Ballantine, D. S.; White, R. M.; Martin, S. J.; Ricco, A. J.; Zellers, E. T.; Frye, G. C.; Wohltjen, H., Eds. *Acoustic wave sensors: theory, design, and physicochemical applications*; Academic Press: San Diego, 1997.
- (5) Kovacs, G.; Venema, A. *Appl. Phys. Lett.* **1992**, *61*, 639–641.
- (6) McHale, G.; Newton, M. I.; Martin, F. *J. Appl. Phys.* **2002**, *91*, 9701–9710.
- (7) Du, J.; Harding, G. L.; Ogilvy, J. A.; Dencher, P. R.; Lake, M. *Sens. Actuators, A* **1996**, *56*, 211–219.
- (8) Gizeli, E. *Smart Mater. Struct.* **1997**, *6*, 700–706.
- (9) Du, J.; Harding, G. *Sens. Actuators, A* **1998**, *65*, 152–159.
- (10) Tom-moy, M.; Baer, R. L.; Solomon, D. S.; Doherty, T. P. *Anal. Chem.* **1995**, *67*, 1510–1516.
- (11) Gizeli, E.; Liley, M.; Lowe, C. R.; Vogel, H. *Anal. Chem.* **1997**, *69*, 4808–4813.
- (12) Harding, G. L.; Du, J.; Dencher, P. R.; Barnett, D.; Howe, E. *Sens. Actuators, A* **1997**, *61*, 279–286.
- (13) Melzak, K.; Gizeli, E. *J. Colloid Interface Sci.* **2001**, *246*.

Obtaining kinetic information about interfacial measurements requires careful analysis. Using an interface for the immobilization of one species of the binding partners may lead to considerable concentration gradients of the other binding partner in solution.² An interface breaks the symmetry of the receptor–ligand complex, so orientation alignment and accessibility of binding sites of the immobilized species may affect the binding parameters. Engineering the surface to have laterally isotropic, homogeneous, and equivalent binding sites is furthermore a challenge.¹⁴ The analyses in this work of binding constant information obtained from surface-sensitive sensors address these issues and are applicable to other biological systems, such as protein interactions on supported lipid bilayers.

This work is focused on using the mass sensitivity of the acoustic waveguide device (see Figure 1) to measure binding constants in a comparative fashion for two immunological reactions: antibody immunoglobulin G (IgG) binding to surface-bound bacterial cell wall proteins, *streptococcal* protein G and *Staphylococcus aureus* protein A. Through diverse interactions with IgG molecules, pathogenic Gram-positive bacterial cell wall-bound receptors such as proteins A and G may play a critical role in the virulence of the bacteria.¹⁵ Primary interest in protein G (MW = 30 000) and protein A (MW = 42 000) is based on their rather unique reactivity with the Fc fragment of immunoglobulins.¹⁶ The earlier discovered and better characterized protein A is known to have distinct types of binding activity: a primary reaction with IgG and other classes of Ig at sites located in the Fc region and a weaker reaction localized to a region outside the antigen combining site.¹⁶ The avidity of protein G for IgG is greater than that of protein A although over a narrower spectrum of Ig classes. Protein G binds monoclonal antibodies from mouse and rat, a property that is poor in protein A, and therefore is considered a more general and versatile IgG binding reagent.¹⁷ Both proteins are known to bind IgG to Fc sites even when the antigen combining sites are occupied. Such properties make these Fc binding reactions of primary interest to immunoassay and chromatography applications. Without competition or complete equilibrium studies, the relative apparent binding strength of each of these two proteins is reported by using two acoustic waveguide devices, one operating at 108 MHz (Q108) and another at 155 MHz (Q155). The methodological strengths of low sample volumes/small experimental time and the challenges in data analysis are addressed.

EXPERIMENTAL SECTION

Materials. Phosphate-buffered saline (PBS) tablets, pH 7.4 (0.01 M phosphate, 2.7 mM potassium chloride, and 0.137 sodium chloride), 2-ethoxyethyl acetate, medium molecular weight poly(methyl methacrylate) (PMMA), glycerol, *streptococcal* protein G, and *S. aureus* protein A were purchased from Sigma. Novolac photoresist was purchased from Shipley. Monoclonal immunoglobulin G, raised against hormone estrone 3-glucuronide (anti-E3G IgG), was obtained from Unilever Research, Colworth, U.K.

Devices. (i) Q108 MHz. A 108-MHz quartz device was fabricated on a 0.5-mm-thick piezoelectric quartz crystal, specif-

- (14) Duschl, C.; Sevin-Landais, A.-F.; Vogel, H. *Biophys. J.* **1996**, *70*, 1985–1995.
- (15) Eliasson, M.; Anderson, R.; Olsson, A.; Wigzell, H.; Uhlen, M. *J. Immunol.* **1989**, *142*, 575–581.
- (16) Langone, J. *Adv. Immunol.* **1982**, *32*, 157–241.
- (17) Bendayan, M.; Garzon, S. *J. Histochem. Cytochem.* **1988**, *36*, 597–607.

ically a rotated Y-cut (42.5°) quartz with propagation 90° with respect to the *x*-axis. The interdigitated transducers, composed of a 210-nm-thick Cr/Au (10/200 nm) electrode, consisted of 80 pairs of split fingers with a periodicity of 45 μm. The path length of the device was 7.21 mm.

(ii) Q155 MHz. A 155-MHz quartz device was fabricated on a 0.5-mm-thick piezoelectric quartz crystal, specifically a rotated Y-cut (42.5°) quartz with propagation 90° with respect to the *x*-axis and composed of 92 electrode pairs. The devices were fabricated with 120-nm-thick Cr/Au (20/100 nm) split finger IDTs having a period of 32 μm. The device utilized a dual delay line configuration where one delay line could act as the reference line and the other as the sensing line. The path length of the device was 5.73 mm.

Novolac Waveguide Deposition. Novolac solution (50% w/w) was applied on Q155 and Q108 device surfaces, respectively, by using a spin coater (Speciality Coating Systems P6700) at 4000 rpm for 40 s. The solvent was evaporated by heating the coated device in an oven at 190 °C for 2 h. The devices were measured before and after coating with the polymer, and the frequency and amplitude changes were recorded. The thickness of the waveguide layer was measured to be 0.9 μm by using a surface profilometer (Dektak).

Instrumentation, Acoustic Measurements, and Data Acquisition. For the Q108-MHz waveguide device, a Hewlett-Packard 4195A network analyzer was used to monitor the frequency and phase of the wave. To minimize interfering reflections, the device was measured with Scotch tape on the back. For the Q155 MHz, a Hewlett-Packard 8753ES network analyzer was used for performing the measurements. The Fourier transform/time gating function of the device was used for biosensing measurements in order to minimize unwanted interference with electromagnetic feed-through and triple transit signals. Acoustic phase measurements were reproducible between the two network analyzers. The insertion loss of the two waveguide devices before liquid loading was ~-30 dB. More information on the frequency spectra and performance of the waveguide geometries can be found in the literature.¹⁸

An HPVEE and VEE software program was used for collecting acoustic data for the Q108- and 155-MHz devices, respectively. Noise in the data introduced by temperature and local electric field drifts in the environment was corrected as follows: the drift in phase for each experiment was linearly fitted and then extrapolated to times when protein solutions were passed over the device. The corrected phase data are, thus, the raw phase measured during protein solution pass minus the extrapolated linear drift. Normalized phase change was also used whenever necessary in order to correct for any differences in the sensitivities between the 108- and 155-MHz devices.

Device Cleaning. Devices were recycled by removing the waveguide polymer layer and depositing a new one. The Novolac-coated devices were treated by soaking them in 4 M sodium hydroxide for at least 1 h and then placing them in a sonicating bath for 20 min in sodium hydroxide followed by distilled water rinse. Then the devices were dipped into freshly prepared and still hot (50 °C) Piranha solution, consisting of sulfuric acid (97%) and hydrogen peroxide (27.5%) in a ratio of 3:1 (v/v), for 5 min.

Gold Surface Preparation. The area between the IDTs on the Novolac- or PMMA-coated device was coated with 10 nm of gold by thermal evaporation at a pressure of less than 5.0×10^{-6} mbar using an Edwards (Auto 306) evaporator. Plasma etching of the surface utilized atmospheric gas at 9.0×10^{-2} – 2.1×10^{-1} mbar for 5 min.

Liquid Loading and Flow. Each device was mounted in a special holder and liquid was pumped through on the area between the IDTs using a peristaltic pump and flow-through cell. The flow cell was sealed on the surface by using a custom-made rubber gasket. Due to the different size of each device, two different flow cells were manufactured by exposing 0.12 and 0.06 cm² of the Q108 and Q155 devices, respectively, to the solution. Flow rates varied between 6 and 83 μL/min among all experiments.

IgG Binding to the Protein G-Modified Device Surface. The plasma-etched gold surface was placed in the device holder and exposed to PBS buffer for ~1 h at a flow rate of 40 μL/min. Protein G at a concentration of 1.7 μM (50 μg/mL) in PBS was added and left in contact with the device surface at the above flow rate for 15 min. Different solutions of monoclonal antibodies raised against estrone 3-glucuronide at a concentration range of 6.7–667 nM (1–100 μg/mL) in PBS were finally added to the device surface followed by buffer rinse.

IgG Binding to the Protein A-Modified Device Surface. The freshly prepared gold surface was placed in the device holder and exposed to PBS buffer for ~1 h at a flow rate of 83 μL/min. Protein A at a concentration of 1.2 μM (50 μg/mL) in PBS was added and left in contact with the device surface at the above flow rate for 30 min. Different solutions of monoclonal antibodies of anti-E3G IgG at a concentration range of 0.7–667 nM (0.1–100 μg/mL) in PBS were finally added to the device surface followed by buffer rinse.

IgG Binding to the Protein G-Modified Surface: Study with Surface Plasmon Resonance. A freshly prepared, plasma-etched gold surface on a glass slide was placed in the Autolab SPR sample holder and exposed to PBS buffer for ~1 h in a static cell. Protein G in a concentration of 50 μg/mL in PBS was added and left in contact with the device surface with intermittent mixing. Following a 2-mL buffer rinse, 150 μL of monoclonal antibodies of anti-E3G at 333 nM in PBS was finally added to the device surface followed by buffer rinse. Surface plasmon resonance (SPR) measurements were performed using an Autolab SPR (Eco Chemie B.V.) instrument.

RESULTS

IgG-Protein G Binding. IgG binding to protein G was determined acoustically by monitoring mass changes on the sensing surface, as these were followed by recording the phase of the wave in real time. The gold surface on top of the polymer waveguide on a Q108 acoustic device was first modified by the adsorption of protein G to produce a biorecognition surface. Figure 2a shows the real-time phase change observed on addition of 50 μg/mL protein G, subsequent PBS buffer rinse, and then IgG binding. Protein G irreversibly adsorbs to the surface since phase mass changes are negligible after the buffer wash. Experiments similar to that shown in Figure 2a were performed for the following IgG concentrations: 6.7, 17, 33, 67, 167, 333, and 667 nM. For all

(18) Gizeli, E.; Bender, F.; Rassmusson, A.; Saha, K.; Josse, F.; Cernosek, R. *Biosens. Bioelectron.*, submitted.

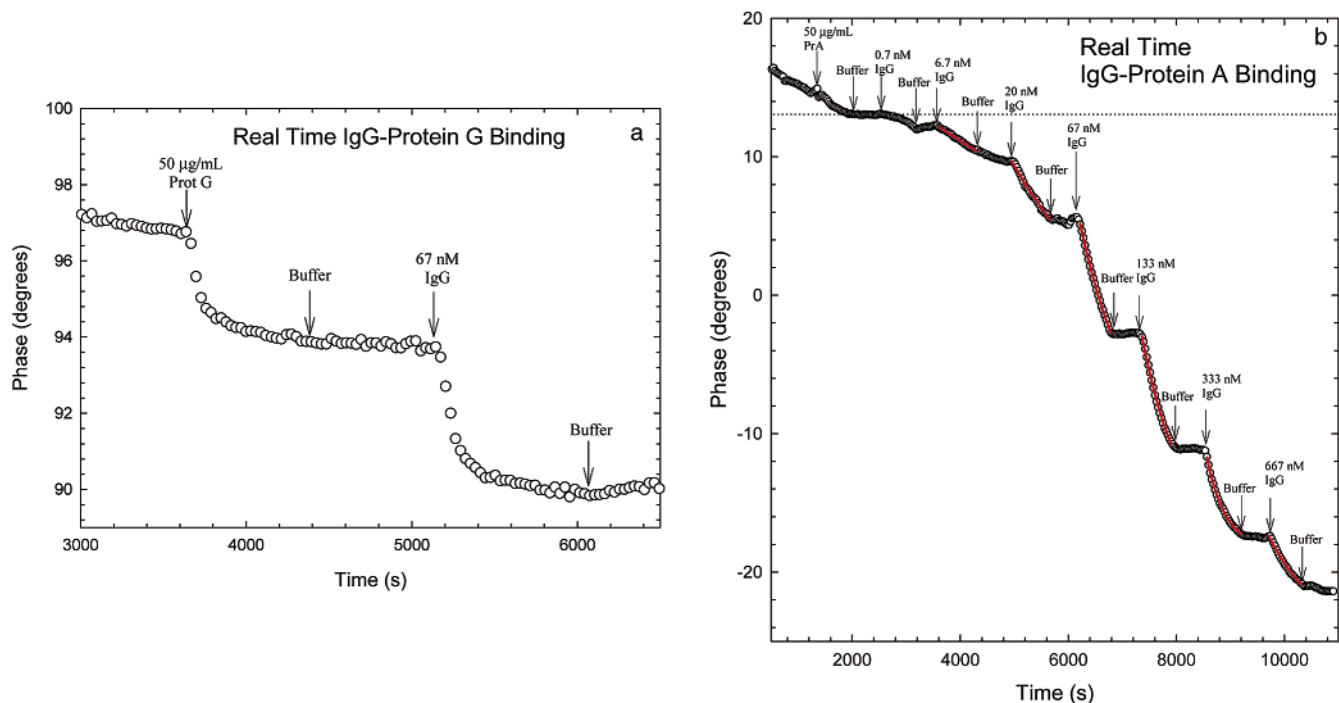


Figure 2. (a) Real-time data during IgG–protein G experiment for 108-MHz quartz device. Sequence of solutions applied: PBS buffer, 50 $\mu\text{g}/\text{mL}$ protein G in PBS buffer, PBS buffer, 67 nM IgG in PBS buffer, and PBS buffer. (b) Real-time data during IgG–protein A experiment for 155-MHz quartz device. Sequence of solutions applied: PBS buffer, 50 $\mu\text{g}/\text{mL}$ protein G, PBS buffer, 0.7 nM IgG, PBS buffer, 6.7 nM IgG, PBS buffer, 20 nM IgG, PBS buffer, 67 nM IgG, PBS buffer, 133 nM IgG, PBS buffer, 333 nM IgG, PBS buffer, 667 nM IgG, and PBS buffer. All solutions in PBS buffer. Solid lines represent three-parameter, single-exponential fits to experimental data (see Discussion).

IgG additions, desorption of IgG during the first 10 min of buffer pass after IgG addition was less than 5%.

IgG–Protein A Binding. IgG binding to protein A was determined by monitoring mass changes on the sensing surface. The gold surface on top of the Novolac waveguide on a Q155 acoustic device was first modified by the adsorption of protein A and then stepwise binding of IgG was performed. Figure 2b shows the phase change observed on addition of 50 $\mu\text{g}/\text{mL}$ protein A, subsequent PBS buffer rinse, and increasing concentrations of IgG added to the surface. Protein A irreversibly adsorbs to the surface since mass changes are negligible after buffer wash. IgG desorption also is negligible during the 10 min of buffer wash after each IgG addition.

DISCUSSION

Kinetics of IgG Binding. Assuming that the experiments are not mass-transfer limited (see Mass-Transfer Considerations section), the binding rates measured represent reaction velocities between IgG and proteins. IgG binding kinetics can be described by the following equation and rate:¹⁹



$$d[\text{IgG:Pr}]/dt = k_a[\text{Pr}][\text{IgG}] - k_d[\text{IgG:Pr}] \quad (2)$$

where IgG is treated as the ligand and Pr is either protein G or A and treated as the receptor. The total protein concentration

$\text{Pr}_{\text{tot}}^{\text{surf}}$ is constant in each experiment and is equal to the sum of the bound and unbound protein surface concentration, i.e., $[\text{Pr: IgG}]$ and Pr , respectively. For the acoustic waveguide device, acoustic phase mass response has been extensively modeled and experimentally tested as being proportional to surface-attached mass.⁶ In these experiments at any given time, acoustic phase, P , is proportional to $[\text{IgG–Pr}]$, so eq 2 becomes

$$dP/dt = k_a(\alpha\text{Pr}_{\text{tot}}^{\text{surf}} - P)[\text{IgG}] - k_dP \quad (3)$$

where α is the device proportionality constant ($\text{degree}/(\text{ng}/\text{cm}^2)$) between surface coverage and acoustic phase, P . Equation 3 is the differential equation that applies for all experiments in this work that follow traditional binding kinetics described in eq 1.

Method of Initial Rates. The method of initial rates was used to estimate the association constant, k_a , for IgG–protein G binding. This method involves measuring the rate of reaction, $d[\text{IgG:Pr}]/dt$, at very short times before any significant changes in concentration occur. The initial concentration of IgG is taken to be that at bulk and IgG:Pr concentration is approximated to be zero for initial times. Therefore, eq 3 reduces to the following in this approximation:

$$dP_o/dt = k_a\alpha\text{Pr}_{\text{tot}}^{\text{surf}}[\text{IgG}]_{\text{bulk}} \quad (4)$$

To estimate the initial reaction rate, dP_o/dt , the phase change over the first ~ 200 s is fitted to a straight line for each IgG concentration applied (e.g., one line used to determine fit shown in Figure 3). Figure 3 indicates the phase changes, after correcting for

(19) Karlsson, R.; Michaelsson, A.; Mattsson, L. *J. Immunol. Methods* **1991**, *145*, 229–240.

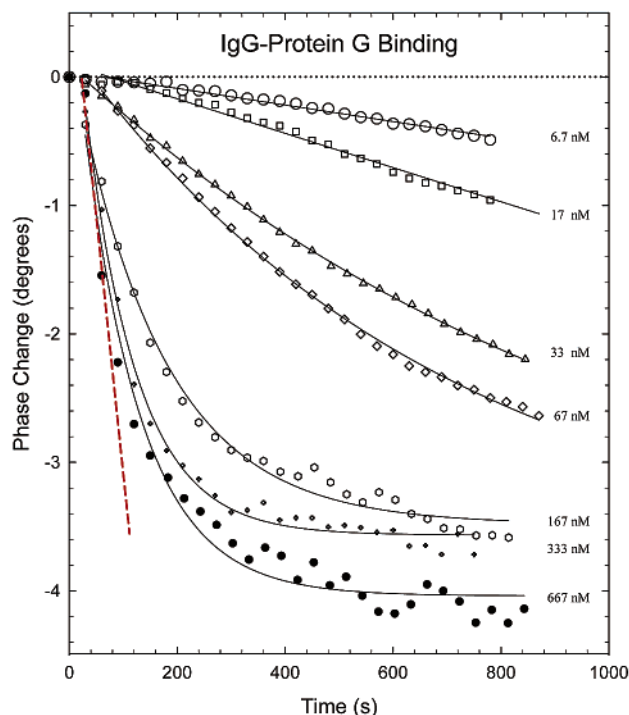


Figure 3. Phase changes during IgG binding from experiments similar to that shown in Figure 2a. All experiments had a protein G sublayer from deposition of 50 $\mu\text{g}/\text{mL}$ protein G on the gold-sensing surface. Solid lines represent three-parameter, single-exponential fits to experimental data. The dashed line represents a fit used for initial rates plotted in Figure 4. Zero on the abscissa is the time at which IgG was added to the device.

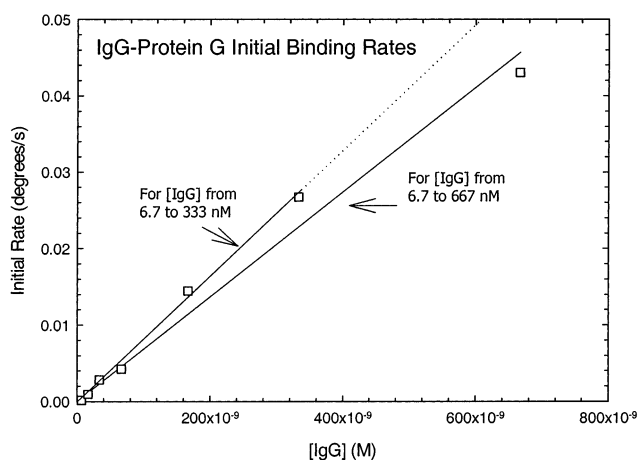


Figure 4. Initial rate plot for determining association constant of IgG–protein G binding. Slopes were calculated using the first ~ 200 s of the plot in Figure 3 for each IgG concentration applied. The two linear regression fits correspond to the including the data for 6.7–667 and 6.7–333 nM range.

systematic noise, during IgG addition only for protein G experiments similar to that shown in Figure 2a. The slopes of the initial rate line fits are plotted in Figure 4. Linear regression of all data in Figure 4 yielded a fit with a slope of $6.65 \times 10^4 \text{ deg M}^{-1} \text{ s}^{-1}$ corresponding to $\alpha k_a \text{Pr}_{\text{tot}}^{\text{surf}}$ from eq 4. The phase equivalent to maximum protein coverage, $\alpha \text{Pr}_{\text{tot}}^{\text{surf}}$, was estimated as that at saturation. Phase change for this acoustic device at saturation was 4.0 deg (Figure 3). Therefore, $\alpha \text{Pr}_{\text{tot}}^{\text{surf}}$ corresponds to 4.0 and the association constant is estimated as $1.7 \times 10^4 \text{ M}^{-1} \text{ s}^{-1}$ by this

method. Binding at 667 nM seems to be an outlier slower than the rest of the data, as is seen in the subsequent analysis as well. Without including binding at 667 nM, for similar initial rate method analysis in the range of 6.7–333 nM, the slope in Figure 4 is $8.2 \times 10^4 \text{ deg M}^{-1} \text{ s}^{-1}$; saturation occurs at 3.6 deg, resulting in $2.3 \times 10^4 \text{ M}^{-1} \text{ s}^{-1}$ for k_a .

Kinetic and Thermodynamic Analysis from Nonequilibrium Data. While the method of initial rates uses an approximation to estimate the association constant, a more sophisticated analysis that uses all the data during binding can be applied for calculation of binding constants. The governing differential equation, eq 3, can be plotted as dP/dt against P giving a straight line with a gradient of

$$\Delta(dP/dt)/\Delta P = k_a[\text{IgG}] + k_d \quad (5)$$

Plotting this gradient, $\Delta(dP/dt)/\Delta P$, versus $[\text{IgG}]$ for the individual measurements at different concentrations, a straight line yielding both kinetic constants should be obtained. To apply this analysis to these data, first the IgG binding at each concentration is fitted to a single-exponential curve as shown in Figures 2b and 3. A single-exponential curve is appropriate for the simple mechanism proposed in eq 1, since the integrated form of eq 3 is a single exponential:

$$P(t) = \frac{k_a[\text{IgG}]\alpha \text{Pr}_{\text{tot}}^{\text{surf}}}{k_a[\text{IgG}] + k_d} - \frac{k_a[\text{IgG}]\alpha \text{Pr}_{\text{tot}}^{\text{surf}} - (k_a[\text{IgG}] + k_d)P_0}{k_a[\text{IgG}] + k_d} e^{-(k_a[\text{IgG}] + k_d)(t - t_0)} \quad (6)$$

where t is time and P_0 is the phase response at time t_0 . For the protein G experiments, P_0 is simply zero, as each IgG concentration was applied to a fresh protein G layer. For protein A experiments, P_0 was the cumulative change in phase since before the first addition of IgG (0.7 nM). Note that the cumulative change calculated from the data in Figure 2b was corrected for linear drift during buffer solution passes before each addition arising from temperature changes and systematic noise. The experimental fit on drift-corrected data was used in the subsequent kinetic analysis.

The plot of $\Delta(dP/dt)/\Delta P$ against $[\text{IgG}]$ is shown in Figure 5. From eq 5, a straight line fit to the data yields a gradient corresponding to k_a and an intercept corresponding to k_d . The results are fitted for the concentrations between 6.7 and 333 nM. As shown in Figure 5, binding at 667 nM is significantly slower than expected from the linear trend of lower concentrations. Binding at 667 nM may follow a different mechanism from that proposed in eq 1 via reactions in non-Fc fragments of the IgG—particularly through the Fab regions of IgG. Protein A is known to have a weaker secondary affinity for the Fab region of certain IgGs.¹⁶ Also, protein G has been suggested to show exclusive specificity for Fab region determinant(s) not recognized by protein A.^{15,20} Cross-reactivity of IgG at high surface concentrations has also been seen in the literature.²¹ For such mechanisms, a more sophisticated fit must be made (e.g., a double-exponential plot), so

(20) Bjorck, L.; Kronvall, G. *J. Immunol.* **1984**, *133*, 969–973.

(21) Weiss, M.; Welsch, W.; Von Schickfus, M.; Hunklinger, S. *Anal. Chem.* **1998**, *70*, 2881–2887.

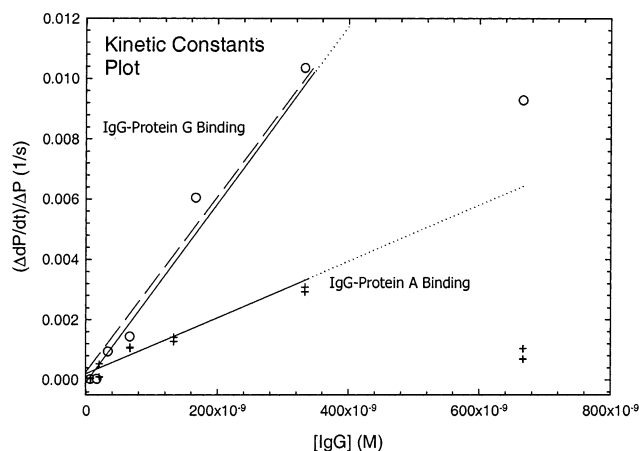


Figure 5. Plot to determine kinetic constants for IgG binding to protein G (o) and protein A (+). Solid lines correspond to linear regression fits for IgG–protein G and IgG–protein A binding between 6.7 and 333 nM. The dashed line is the fit using initial rate slope from Figure 4 for IgG–protein G between 6.7 and 333 nM.

Table 1. Summary of Apparent Binding Constants from Kinetic Analysis of Nonequilibrium Binding Data

binding system	k_a ($M^{-1}s^{-1}$)	k_d (s^{-1})	K (M^{-1})
IgG–protein G	3.29×10^4	2.90×10^{-4}	1.13×10^8
IgG–protein A	8.02×10^3	2.77×10^{-4}	2.90×10^7

the $\Delta(dP/dt)/\Delta P$ from the simple single-exponential fit has a different interpretation. In the range of 6.7–333 nM, the association constants (k_a) obtained from Figure 5 are 3.29×10^4 and $8.02 \times 10^3 M^{-1} s^{-1}$ for IgG–protein G and IgG–protein A, respectively. For IgG–protein G, good agreement between this k_a determination and the estimate from initial rates ($2.3 \times 10^4 M^{-1} s^{-1}$) is seen. Linear regression to IgG–protein G data yielded a negative intercept, and instead, a straight line fit for protein G data with a slope of $2.3 \times 10^4 M^{-1} s^{-1}$ from initial rates for 6.7–333 nM IgG was used to obtain an intercept of 2.90×10^{-4} , the k_d . A summary of all results is shown in Table 1.

Comparison of values in Table 1 between proteins is consistent with the literature. Literature equilibrium constant (K) values for solution-phase IgG–protein A binding are between 4.6×10^7 and $2.0 \times 10^8 M^{-1}$.¹⁶ Protein G has been seen to have a higher affinity for IgG with 2–4 times more binding occurring at equilibrium in comparative studies.²² On immobilized systems, protein G has been shown to have more than 5 times more reactivity at equilibrium than protein A.²³ Higher k_a and K determined for protein G support these previous general findings.

Comparison to Equilibrium Studies. It is common practice to determine thermodynamic constants (K) of binding reactions by using equilibrium-based Langmuir isotherms and calculating K by taking the inverse at the concentration at which half of maximal binding occurs. To investigate whether there is any advantage in calculating K by using the nonequilibrium approach described in the previous section over the Langmuir isotherm one, the two methods are compared.

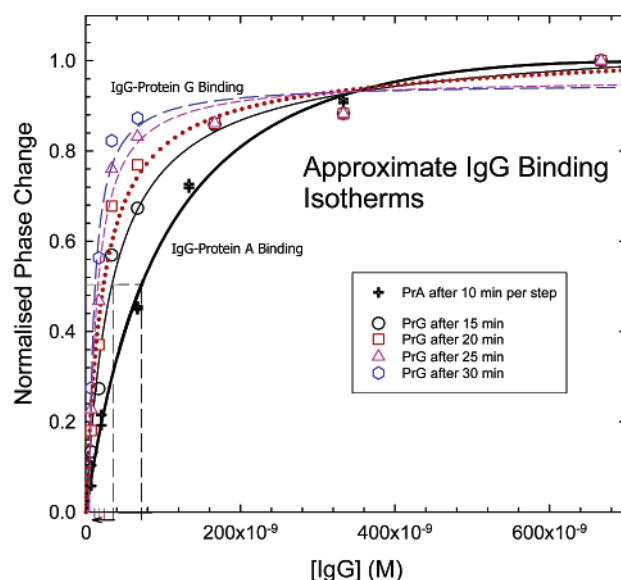


Figure 6. Approximate binding isotherms for IgG binding. IgG–protein A results are for stepwise binding as in Figure 2b. IgG–protein G are shown for 15 min and for 20, 25, and 30 min based on extrapolated fits to data. All phase changes are normalized by the phase change at 667 nM for differences due to frequency of operation.

In the experiments shown in Figures 2b and 3, reaction times were restricted by buffer pass before equilibrium was reached. To illustrate how far from equilibrium the binding was when the reaction was stopped, an approximate binding isotherm was determined for both IgG–protein G and IgG–protein A binding reactions (Figure 6). Since reaction times are restricted in those experiments, the curves shown in Figure 6 are only approximations to the true equilibrium isotherm that should be seen at very long times.¹⁶ In Figure 6, IgG–protein A changes are cumulative for stepwise binding as shown in Figure 2b. IgG–protein G plots are for 15 min from Figure 3 and for 20, 25, and 30 min based on extrapolated exponential fits to data in Figure 3. Note that the concentration at which saturation occurs moves to lower concentrations with increasing time. Fifteen minutes is clearly not enough time for equilibrium to be established for low concentrations. More than 30 min is most likely needed for equilibrium to be established for concentrations lower than 100 nM.

By calculating the inverse at the concentration at which half of maximal binding occurs (0.5 on the ordinate of Figure 6), the K estimate for IgG–protein A was calculated to be $1.4 \times 10^7 M^{-1}$ (1/71 nM), which is lower than the K of $2.9 \times 10^7 M^{-1}$ derived from the kinetic analysis. For binding to protein A at low concentrations, the reaction is definitely far from equilibrium after 10-min steps (see Figure 2b), indicating that the estimate from the approximate adsorption isotherm in Figure 6 will be too low. From the K of IgG–protein G analysis, K estimates are 2.9×10^7 (1/34 nM), 4.6×10^7 (1/22 nM), 6.4×10^7 (1/16 nM), and $9.1 \times 10^7 M^{-1}$ (1/11 nM) for isotherms after 15, 20, 25, and 30 min, respectively. The trend of higher K for longer times, or allowing the reaction to come closer to equilibrium, is consistent with the supposition of approaching the true equilibrium K predicted from kinetic analysis ($1.13 \times 10^8 M^{-1}$).

The above analysis indicates that the Langmuir isotherm can be used to derive K values of a binding reaction only if a true equilibrium has been reached. In contrast, the kinetic analysis

(22) Akerstrom, B.; Brodin, T.; Reis, K.; Bjorck, L. *J. Immunol.* **1985**, *135*, 2589–2592.

(23) Suri, C.; Mishra, G. *Biosens. Bioelectron.* **1996**, *11*, 1199–1205.

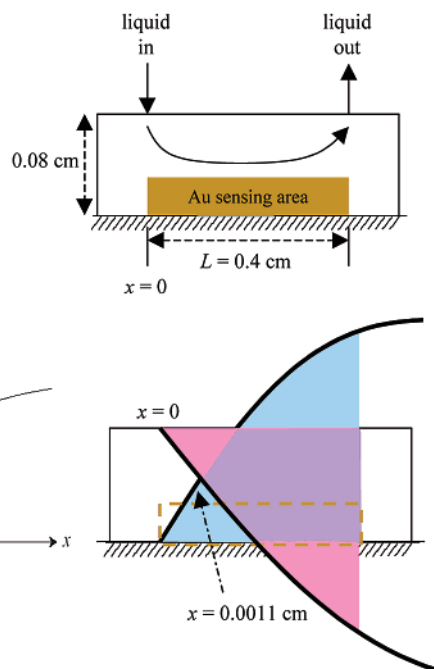


Figure 7. Schematic of liquid flow cell with overlapping developing boundary layer schematic. Boundary layer shown for laminar flow in the middle of sensing area. δ is the boundary layer thickness. Drawing not to scale.

applied in this work illustrates that both kinetic and equilibrium constants can be obtained in half of the time required for establishing equilibrium. Such an advantage is a clear strength of this detection method and analysis whereby binding constants of biological interactions are performed much faster and in lower sample volumes.

Mass-Transfer Considerations. Since reaction parameters are of interest measuring the reaction rate, and not simply the rate at which ligands arrive to the surfaces, must be ensured. Flux of ligands at any point can be described by

$$N_{\text{IgG}} = k([\text{IgG}] - [\text{IgG}]_{\text{surf}}) \quad (7)$$

where molar flux N_{IgG} is measured relative to a set of axes fixed in space, $[\text{IgG}]_{\text{surf}}$ is the IgG concentration at a solid surface, $[\text{IgG}]$ is the IgG concentration at some arbitrarily defined point in the fluid medium, and k is the overall mass-transfer coefficient (also called the Onsanger coefficient). Equation 7 is a generalized engineering form of Fick's law, where the driving force is the concentration gradient between the phase boundary and bulk. The mass-transfer coefficient describes the overall *form* and *length scale* over which the gradient occurs. It is interpreted as the resistance of motion of a species between the bulk and the surface. For example, for a static medium between the bulk concentration and surface, k is equal to the diffusion coefficient divided the thickness of the static medium. Analogously in flow situations, there is a thin static medium at surfaces called the "boundary" layer (Figure 7). In this layer, the velocity and concentration of a species changes from that in the bulk of the solution to that at the surface. Flow conditions and geometry of the surface strongly affect the thickness of this boundary layer, which correspondingly affects the mass-transfer resistance of a species from the bulk to

Table 2. Comparison of Mass-Transfer and Reaction Rates for IgG–Protein G Binding

[IgG] applied to protein G layer (nM)	N_{IgG} , mass-transfer rate estimate ($\text{ng cm}^{-2} \text{s}^{-1}$)	initial reaction rate ($\text{ng cm}^{-2} \text{s}^{-1}$)
6.7	0.066	0.012
16.7	0.17	0.071
33.3	0.33	0.20
66.7	0.66	0.27
166.7	1.7	0.93
333.3	3.3	1.7
666.7	6.6	3.0

the surface. Boundary layer thickness as given by traditional fluid dynamics (see Appendix for calculations) was seen to be far larger than the thickness of the flow chamber (>0.08 cm as shown in Figure 7). In such a complex flow regime of boundary layers combining within the flow, microfluidic considerations must be made. Microfluidic considerations are very geometry dependent and must be calculated numerically. Instead, we use a simple approximation to estimate a lower limit of mass transfer is such a flow profile: laminar flow at the same velocity over a flat plate (i.e., the case when there is no top boundary in the flow cell). A numerical analysis of similar systems has already been described in the literature.²⁴

A summary of mass-transfer rates at IgG different concentrations through our approximation (see Appendix for calculations) is listed in Table 2. The mass-transfer coefficients in our calculations agreed well with published data²⁴ and were in the same order of magnitude. Comparison to the maximum reaction rates is achieved from the initial rates plotted in Figure 4. Rates in Figure 4 are in units of degrees, so calibration of mass sensitivity to protein coverage was done by performing SPR measurements of IgG–protein G. SPR measurements indicated that 236 ± 67 ng/cm² binding occurs at 333 nM IgG concentration. A 3.6° phase response is measured with the device at the same concentration. Therefore, every 3.6° is 236 ± 67 ng/cm², and data in Figure 4 can be interpreted in terms of reaction rates.

Table 2 indicates that the estimate for mass transfer is faster than the reaction rate. These mass-transfer rates occurring over a flat plate are for mass transfer over laminar flow velocity profile and concentration gradient within the thickness of the flow cell (0.08 cm). In the flow cell, the gradients will be larger, because the length scale over which mass transfer must occur is smaller—boundary layer in the flow must be less than the flow cell thickness (0.08 cm). Larger gradients necessarily imply faster mass transfer. Furthermore, there is significant turbulent flow near the entrance regions ($x < 0.0011$ in Figure 7), which is known to promote mixing and enhance mass transfer. While IgG–protein A binding is almost 1 order of magnitude slower ($k_a^{\text{PrA}} < k_a^{\text{PrG}}$), mass transfer will occur faster since experiments occur at double the flow rate in the protein A case. Based on the above, mass transfer does not influence the results, since the device measures the slower reaction rate of IgG, the rate of interest in kinetic studies.

CONCLUSIONS

The binding constants for IgG–protein G and IgG–protein A were determined with the acoustic waveguide sensor. Real-time

(24) Glaser, R. *Anal. Biochem.* **1993**, *213*, 152–161.

data in the range of 6.7–333 nM IgG during IgG–protein G and IgG–protein A binding yielded apparent association constants of 3.29×10^4 and $8.02 \times 10^3 \text{ M}^{-1} \text{ s}^{-1}$, leading to apparent equilibrium constants 1.13×10^8 and $2.90 \times 10^7 \text{ M}^{-1}$, respectively. The higher measured rate constants of protein G are consistent with literature equilibrium competition studies. The kinetic analysis of real-time data provided valid, valuable results for both stepwise binding experiments with protein A and individual binding experiments with protein G—both performed without reaching equilibrium for every IgG concentration added. Furthermore, evidence for saturation of protein binding through the Fc region on IgG is seen to occur below 333 nM. The design and flow of the device enables fast mass transfer, allowing quick kinetic measurements with low sample volumes. Comparative, nonequilibrium studies of IgG–protein G and A binding at a solid–liquid interface using the acoustic waveguide device have yielded quantitative kinetic information about the two binding mechanisms.

ACKNOWLEDGMENT

The authors thank Dr. K. Melzak for fruitful discussions and Unipath, Colworth, U.K. for donating the antibodies used in this work. We gratefully acknowledge the financial support of BBSRC and the U.S. Winston Churchill Foundation.

APPENDIX

Mass transfer is sensitive to velocity in the flow direction, v_x (Figure 7), and for our geometry is simply the flow rate divided by the cross-sectional area. With flow rate at $40 \mu\text{L}/\text{min}$ and cross-sectional area of $0.08 \text{ cm} \times 0.391 \text{ cm}$, v_x was $0.021 \text{ cm}/\text{s}$. The Reynolds number (Re) in the flow direction is given by

$$Re_x = \rho v_x x / \eta \quad (\text{A1})$$

where ρ is the density of flowing medium and η is the viscosity of flowing medium. At the end of the flow cell, with $v_x = 0.021 \text{ cm}/\text{s}$, $\rho = 1.0 \text{ g}/\text{cm}^3$, $\eta = 0.01 \text{ g}/\text{cm s}$, and $L = 0.391 \text{ cm}$, $Re_L = 0.81$. For such low Re , flow is laminar.

Using the Blasius approximation,²⁵ the thickness of the boundary layer for laminar flow, $\delta(x)$, at both boundaries at a certain distance x from the entrance of the flow is calculated (shown schematically in Figure 7):

$$\delta(x) = 1.72x(Re_x^{-0.5}) \quad (\text{A2})$$

At the end of the flow cell, the boundary layer thickness, $\delta(L)$, is 0.75 cm .

A simple approximation to estimate a lower limit of mass transfer is used: laminar flow at the same velocity over a flat plate (the case when there is no top boundary in the flow cell). For laminar flow over a flat plate, the following correlation²⁵ allows determination of mass-transfer coefficient, k :

$$Sh = 0.664Re_L^{0.5} Sc^{0.33} \quad (\text{A3})$$

With $Re_L = 0.81$ and Schmidt number (Sc) = $(0.01 \text{ g}/\text{cm s}) / (1 \text{ g}/\text{cm}^3 \times 1.0 \times 10^{-7} \text{ cm}^2/\text{s})$, Sherwood number (Sh) = 28. Using the definition of Sh and scaling by the constrained boundary layer thickness imposed by the flow cell thickness, h , we use the following equation to find the mass-transfer coefficient:

$$k = \frac{Sh \times D}{L} \left(\frac{\delta(L)}{h} \right) \quad (\text{A4})$$

With $Sh = 28$, $D = 1.0 \times 10^{-7} \text{ cm}^2/\text{s}$, $\delta(L) = 0.75 \text{ cm}$, and $h = 0.08 \text{ cm}$, $k = 6.6 \times 10^{-5} \text{ cm}/\text{s}$.

Inserting $k = 6.6 \times 10^{-5} \text{ cm}/\text{s}$ into eq 7, we can easily find the mass flux to the surface for each concentration (e.g., for $[\text{IgG}] = 66.7 \text{ nM}$ and $MW = 150\,000$, $N_{\text{IgG}} = 0.66 \text{ ng}/\text{cm}^2 \text{ s}$).

Received for review July 29, 2002. Accepted November 20, 2002.

AC0204911

(25) Welty, J. R. *Fundamentals of momentum, heat, and mass transfer*, 4th ed.; John Wiley: New York, 2001.